Organic & Biomolecular Chemistry

ROYAL SOCIETY OF CHEMISTRY

PAPER

View Article Online
View Journal | View Issue

Check for updates

Cite this: *Org. Biomol. Chem.*, 2023, **21**, 4661

Human serum albumin-based supramolecular host–guest boronate probe for enhanced peroxynitrite sensing†

He Tian Jr., ‡[a] Chen Guo, ‡[a] Xi-Le Hu, [a] Jing-Bo Wang, [a] Yi Zang, *[c,f] Tony D. James, *[d,e] Jia Li *[c] and Xiao-Peng He *[a,b]

Received 24th April 2023,
Accepted 9th May 2023

DOI: 10.1039/d3ob00637a

rsc.li/obc

Peroxynitrite ($ONOO^-$) is an important oxygen/nitrogen reactive species implicated in a number of physiological and pathological processes. However, due to the complexity of the cellular micro-environment, the sensitive and accurate detection of $ONOO^-$ remains a challenging task. Here, we developed a long-wavelength fluorescent probe based on the conjugation between a TCF scaffold and phenylboronate; the resulting conjugate is capable of supramolecular host–guest assembly with human serum albumin (HSA) for the fluorogenic sensing of $ONOO^-$. The probe exhibited an enhanced fluorescence over a low concentration range of $ONOO^-$ (0–9.6 μM), whist the fluorescence was quenched when the concentration of $ONOO^-$ exceeded 9.6 μM. In addition, when human serum albumin (HSA) was added, the initial fluorescence of the probe was significantly enhanced, which enabled the more sensitive detection of low-concentrations of $ONOO^-$ in aqueous buffer solution and in cells. The molecular structure of the supramolecular host–guest ensemble was determined using small-angle X-ray scattering.

Open Access Article. Published on 22 May 2023. Downloaded on 12/6/2025 5:08:20 AM.
This article is licensed under a Creative Commons Attribution 3.0 Unported Licence.

1. Introduction

Peroxynitrite ($ONOO^-$) is a highly reactive molecule that is formed by the reaction of nitric oxide (NO) and the superoxide anion ($O2^{\bullet-}$).[1] It is involved in various physiological and pathological processes, including inflammation, oxidative stress, and cell death. $ONOO^-$ can react with lipids, proteins, and DNA, leading to cellular damage and dysfunction.[2] In disease development, $ONOO^-$ has been implicated in a wide range of conditions, including cardiovascular disease, neurodegenerative disorders, and cancer.[3] During cardiovascular disease, $ONOO^-$ contributes to the development of atherosclerosis by promoting endothelial dysfunction and lipid oxidation,[4] and in neurodegenerative disorders, $ONOO^-$ is thought to play a role in neuronal damage and death through protein nitration and mitochondrial dysfunction.[5] In addition, $ONOO^-$ has been shown to promote tumor growth and metastasis by inducing DNA damage and activating signalling pathways that facilitate cell survival and proliferation.

Research has indicated that high concentrations of $ONOO^-$ are associated with various diseases such as cardiovascular disease, neurodegenerative diseases, inflammation and cancer.[6] While low concentrations of $ONOO^-$ are required to modulate cellular signalling pathways, a deficit in $ONOO^-$ may lead to immune deficiency and increase susceptibility to infection.[7] Therefore, the development of analytical tools that are sensitive to the dynamic concentration changes of $ONOO^-$ during various biological and pathological processes will facilitate a deeper understanding of ROS/RNS biology and provide tools for disease diagnosis. Conventional techniques for $ONOO^-$ detection include microchip electrophoresis,[8] chromatographic methods utilizing electron spin resonance spectroscopy and Liquid Chromatography Mass Spectrometry,[9] bioluminescent probes,[10] photoacoustic probes,[11] chemiluminescent probes,[12] modified carbon quantum dots,[13] and reaction-based fluorescent probes.[14,15]

The development of fluorescent probes for $ONOO^-$ sensing has proven to be effective to help improve our understanding

[a]*Key Laboratory for Advanced Materials and Joint International Research Laboratory of Precision Chemistry and Molecular Engineering, Feringa Nobel Prize Scientist Joint Research Center, School of Chemistry and Molecular Engineering, East China University of Science and Technology, 130 Meilong Rd., Shanghai 200237, China. E-mail: xphe@ecust.edu.cn*
[b]*National Center for Liver Cancer, The International Cooperation Laboratory on Signal Transduction, Shanghai 200438, China*
[c]*National Center for Drug Screening, State Key Laboratory of Drug Research, Shanghai Institute of Materia Medica, Chinese Academy of Sciences, 189 Guo Shoujing Rd., Shanghai 201203, P. R. China. E-mail: jli@simm.ac.cn*
[d]*Department of Chemistry, University of Bath, Bath, BA2 7AY, UK. E-mail: t.d.james@bath.ac.uk*
[e]*School of Chemistry and Chemical Engineering, Henan Normal University, Xinxiang 453007, China*
[f]*Lingang laboratory, Shanghai 201203, China. E-mail: yzang@simm.ac.cn*

†Electronic supplementary information (ESI) available: Experimental section, additional figures and original spectral copies of new compounds. See DOI: https://doi.org/10.1039/d3ob00637a

‡Equal contribution.

Open Access Article. Published on 22 May 2023. Downloaded on 12/6/2025 5:08:20 AM.
This article is licensed under a Creative Commons Attribution 3.0 Unported Licence.

of its intrinsic roles in complicated biological systems.[16,17] The probes developed have achieved the visualization of $ONOO^-$ in living cells and tissues, allowing researchers to study $ONOO^-$ relevant biological events in real-time.[18] They can also be used to quantify $ONOO^-$ levels in biological samples, thus facilitating the diagnosis of diseases associated with $ONOO^-$. Fluorescent probes targeting $ONOO^-$ typically consist of a fluorophore that is coupled to a specific chemical moiety that reacts with ONOO.[19,20] Upon reaction with $ONOO^-$, the fluorophore undergoes a change in fluorescence intensity or spectral properties, allowing $ONOO^-$ to be detected and quantified. Several types of fluorescent probes have been developed for $ONOO^-$ detection, including aryl boronate-based probes, α-ketoamide-based probes and isatin-based probes.[21–23] However, because small-molecule probes can be unstable in complicated biological systems, supramolecular strategies to enhance their sensing properties have recently been developed.[24]

We have demonstrated that human serum albumin (HSA) is an effective, biocompatible host material to enhance the sensitivity of small-molecule fluorescent probes.[20,25–27] Here, we extended this strategy to improve the sensing ability of a TCF (2-(3-cyano-4,5,5-trimethylfuran-2(5*H*)-ylidene) malononitrile)-based long-wavelength $ONOO^-$ probe. The probe was synthesized through the conjugation between the TCF scaffold and phenylboronate (Fig. 1a). The resulting conjugate is capable of host–guest assembly with HSA exhibiting an enhanced sensitivity for low-concentrations of $ONOO^-$ in aqueous buffer solution and in cells; however, when high concentrations of $ONOO^-$ are added, the fluorescence of the probe is quenched due to structural degradation (Fig. 1b). The molecular structure of the supramolecular ensemble between the probe and HSA was determined using small-angle X-ray scattering (SAXS).

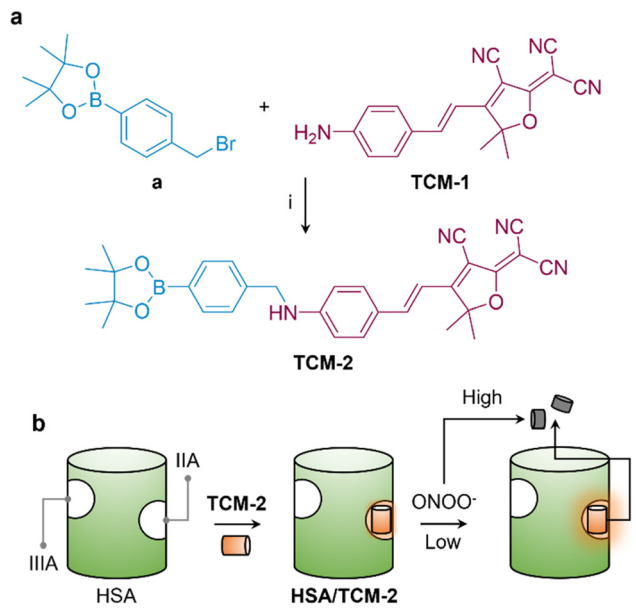

Fig. 1 (a) Synthesis of the peroxynitrite ($ONOO^-$) probe **TCM-2** *via* the conjugation between a and **TCM-1**; reagents and conditions (i): K_2CO_3 in DMF. (b) Schematic illustration of the host–guest inclusion of **TCM-2** into the **IIA** domain of human serum albumin (HSA) for the enhanced fluorogenic sensing of $ONOO^-$; when treated at a low concentration range, the fluorescence of **TCM-2** included in HSA was significantly enhanced, while the fluorescence of the probe was quenched when the concentration of $ONOO^-$ further increases due to structural degradation.

2. Results and discussion

The fluorogenic probe was developed based on a known donor–acceptor (D–A) type fluorescent dye, **TCM-1** was synthesized by the aldol reaction between 2-(3-cyano-4,5,5-trimethylfuran-2(5*H*)-ylidene) malononitrile and 4-aminobenzaldehyde (Scheme S1†).[28] Then, a phenylboronate, which is a known reactive group for $ONOO^-$,[29] was introduced to the amino end of **TCM-1** to produce **TCM-2** with quenched fluorescence due to inhibited intramolecular charge transfer.[30]

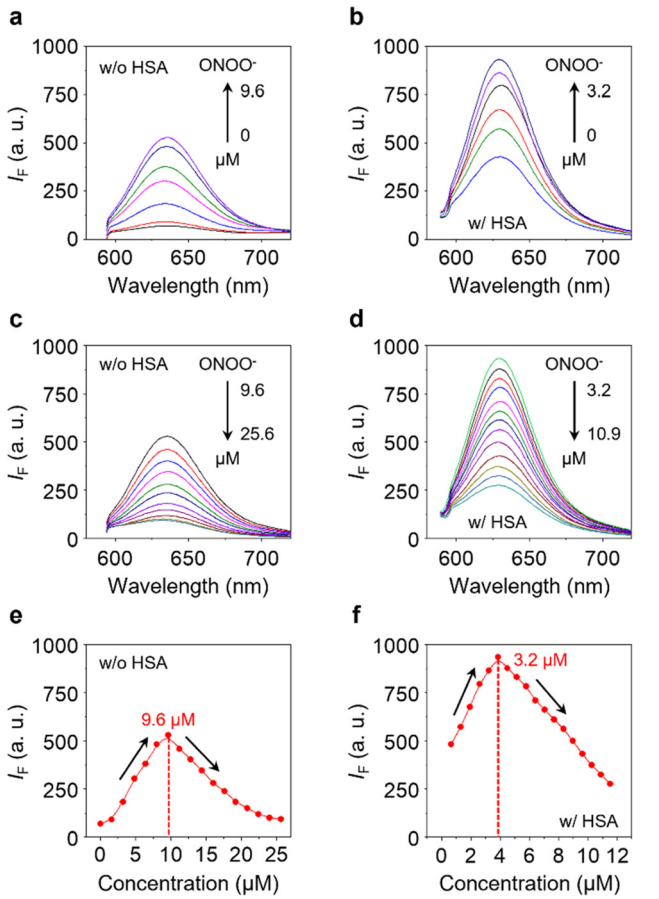

Fig. 2 Fluorescence emission spectra of **TCM-2** (5 μM) with increasing concentrations of $ONOO^-$ ranging from (a) 0–9.6 μM, and (b) 9.6–25.6 μM. Fluorescence emission spectra of **HSA/TCM-2** (10 μM/5 μM) with increasing concentrations of $ONOO^-$ ranging from (c) 0–3.2 μM, and (d) 3.2–10.9 μM. Plot of the fluorescence intensity changes of (e) **TCM-2** (5 μM) and (f) **HSA/TCM-2** (10 μM/5 μM) as a function of $ONOO^-$ concentration. All measurements were performed in phosphate buffered saline (PBS) (0.01 M, pH 7.4, containing 1% DMSO v/v) with an excitation wavelength of 560 nm.

This journal is © The Royal Society of Chemistry 2023

Open Access Article. Published on 22 May 2023. Downloaded on 12/6/2025 5:08:20 AM.
This article is licensed under a Creative Commons Attribution 3.0 Unported Licence.

After reacting with $ONOO^-$, the boronate moiety is removed, resulting in fluorescence recovery of the probe.

With the probe in hand, we evaluated the fluorescence changes in the presence of increasing concentrations of $ONOO^-$ in an aqueous solution. We found a concentration-dependent fluorescence enhancement of the probe with $ONOO^-$ over a concentration range of 0–9.6 μM (Fig. 2a). However, when the concentration continued to increase (9.6–25.6 μM), the fluorescence of the probe gradually decreased (Fig. 2c). In its UV-vis spectrum, we also observed a slightly enhanced absorption peak of **TCM-2** at ~560 nm when the concentration of $ONOO^-$ increased from 0–9.6 μM; however, this peak began to decrease gradually when the concentration of $ONOO^-$ increased from 9.6–25.6 μM (Fig. S1a†). In contrast, the other absorption peak of the probe at ~340 nm enhanced gradually over the entire concentration range of $ONOO^-$ (0–25.6 μM).

We envisioned that the enhanced fluorescence of **TCM-2** with low concentrations of $ONOO^-$ was a result of the removal of the phenylboronate group, thus releasing the **TCM-1** scaffold. To confirm this hypothesis, mass spectroscopic (MS) analysis was used to determine the mass shift of **TCM-2** after treatment with 9.6 μM of $ONOO^-$. As expected, the mass peak assigned to **TCM-1** at *m*/*z* 302.1169 was detected (Fig. S2†). We further envisioned that when the concentration of $ONOO^-$ continues to increase, the structure of **TCM-1** degraded. Indeed, using a tandem liquid chromatograph-mass spectrometer, we found the mass peak of a product of **TCM-1** with one of the cyano groups having been oxidized (1, Fig. S3†); a further oxidatively cleaved product from **TCM-1** was also detected (2, Fig. S3†). In addition, the UV-vis absorption at 512 nm and 350 nm of **TCM-1** gradually decreased and increased with increasing concentrations of $ONOO^-$ (9.6–25.6 μM), respectively (Fig. S1b†), and the fluorescence of **TCM-1** also diminished gradually when 9.6–25.6 μM of $ONOO^-$ was added (Fig. S1c†). These findings collectively suggest that the gradually quenched fluorescence of **TCM-2** at higher concentrations of $ONOO^-$ is the result of structural cleavage. Notably, a previous report also demonstrated the cleavage of the alkenyl bond of TCM-based dyes in the presence of strong oxidants.[31]

Next, HSA was used for host–guest assembly with **TCM-2** under mild sonication (100 W), producing the supramolecular **HSA/TCM-2** ensemble. We first determined that increasing the

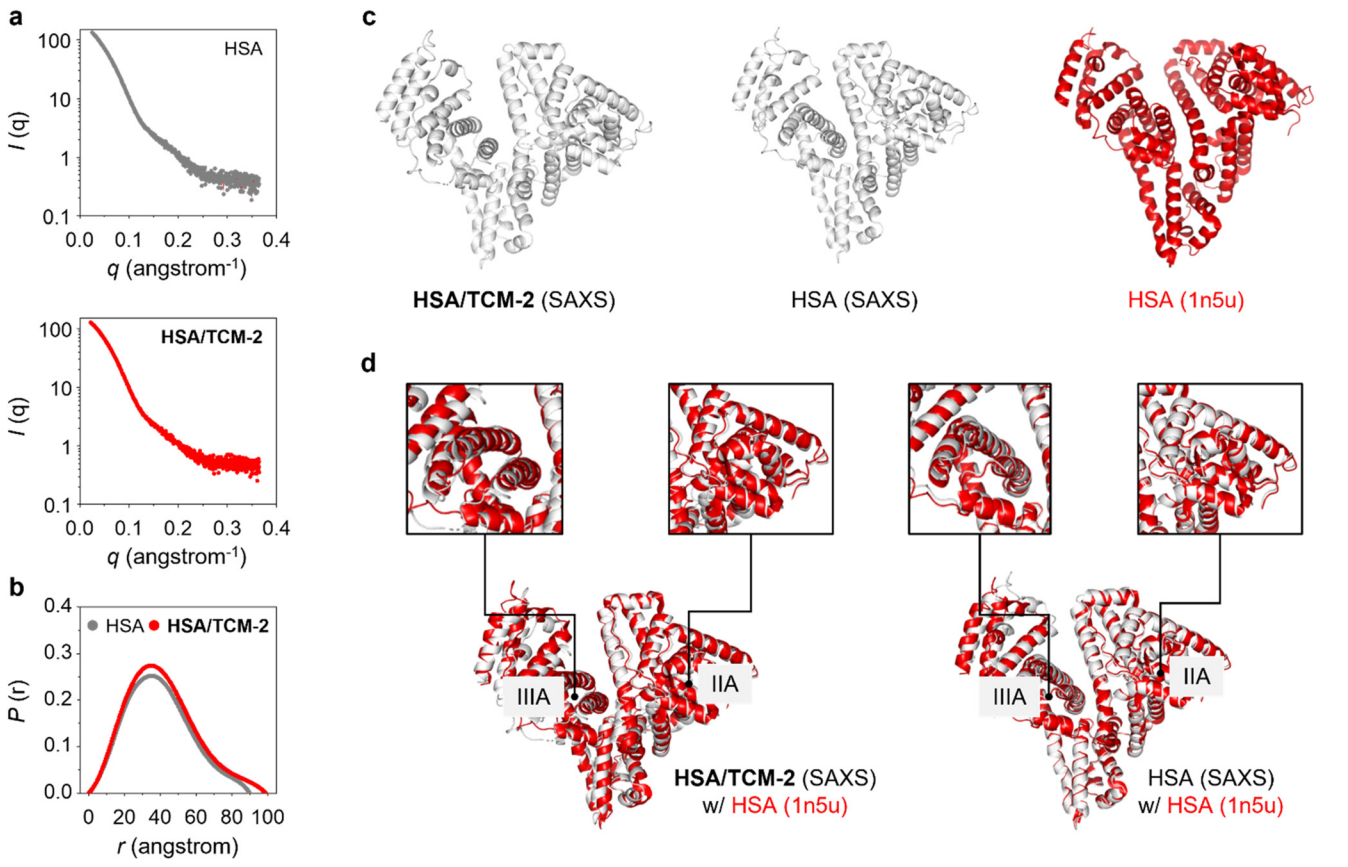

Fig. 3 (a) Small-angle X-ray scattering (SAXS) pattern of HSA and **HSA/TCM-2**. (b) Stacked interatomic distance distribution function, *P*(*r*), of the SAXS patterns of HSA and **HSA/TCM-2**. (c) Atomic models of **HSA/TCM-2** and HSA refined with the scattering data obtained and a known crystal model of HSA (1n5u) extracted from the protein data bank. (d) Superimposed SAXS model of **HSA/TCM-2** and HSA (light grey) with the crystal model of HSA (1n5u, red); the **IIA** and **IIIA** domains of the superimposed models are enlarged to better illustrate the conformational change of HSA after including **TCM-2**.

Open Access Article. Published on 22 May 2023. Downloaded on 12/6/2025 5:08:20 AM.
This article is licensed under a Creative Commons Attribution 3.0 Unported Licence.

concentration of HSA caused the fluorescence of **TCM-2** to enhance gradually (Fig. S4a†), and the fluorescence enhancement is also time-dependent (Fig. S4b†). This observation agrees with previous reports showing that the fluorescence of D–A type fluorogens is enhanced when bound to HSA probably due to a reduction of aggregation-caused quenching and/or an inclusion into the hydrophobic cavity of the protein.[20,32–34] The **HSA/TCM-2** ensemble exhibited concentration-dependent fluorescence enhancement when low concentrations of $ONOO^-$ were added (0–3.2 μM) (Fig. 2b), and the fluorescence began to quench when the concentration exceeded 3.2 μM (Fig. 2c). Interestingly, the fluorescence of **HSA/TCM-2** enhanced more dramatically than that of **TCM-2** over a smaller concentration range of $ONOO^-$ (Fig. 2e *vs.* Fig. 2f). The quenching point of the supramolecular ensemble (3.2 μM) was also 3-fold smaller than that of the probe (9.6 μM). This suggests that the host–guest inclusion of the probe into HSA enhances its reactivity with $ONOO^-$ to first remove the phenylboronate group and then induce the structural degradation. Indeed, the limit of detection of **HSA/TCM-2** for $ONOO^-$ (0.39 nM) was determined to be ~2-fold smaller than that of **TCM-2** (0.84 nM) (Fig. S5†). A thorough comparison to previously developed fluorescent probes for $ONOO^-$ detection suggests that our supramolecular system with host and guest assembly is among the most sensitive (Table S1†).

To determine the binding manner of the probe with HSA, SAXS was used. The scattering signals for HSA in the absence and presence of **TCM-2** were obtained (Fig. 3a), and then the corresponding interatomic distance distribution functions ($P(r)$) were determined (Fig. 3b). We found that the maximum dimension of HSA (89.5 Å) increased to 98.4 Å when **TCM-2** is included. This suggests a conformational change of the protein after binding with the probe. Subsequently, the 3D structures of HSA and **HSA/TCM-2** were simulated and compared to a known crystal structure of HSA (1n5u) extracted from the protein data bank in order to identify the binding site of the probe (Fig. 3c). Shown in Fig. 3d are the superimposed SAXS models of **HSA/TCM-2** and HSA (light grey) with the crystal model of HSA (red). We observed a significant conformational change in the **IIA** domain of the SAXS model of **HSA/TCM-2** with respect to the crystalline HSA structure used as control; a 2.067 Å root-mean-square deviation (RMSD) between the two models was determined. In addition, minimal conformational change was seen for the **IIIA** domain of the SAXS model of HSA, which is also known as a host site for hydrophobic molecules. In contrast, a much greater overlap between the SAXS and crystal model of HSA was seen with a RMSD of 0.743 Å. A subsequent competition assay using known **IIIA** and **IIA** binding agents corroborates that the probe is included into the **IIA** region of HSA (Fig. S6†). The supramolecular **HSA/TCM-2** probe also dis-

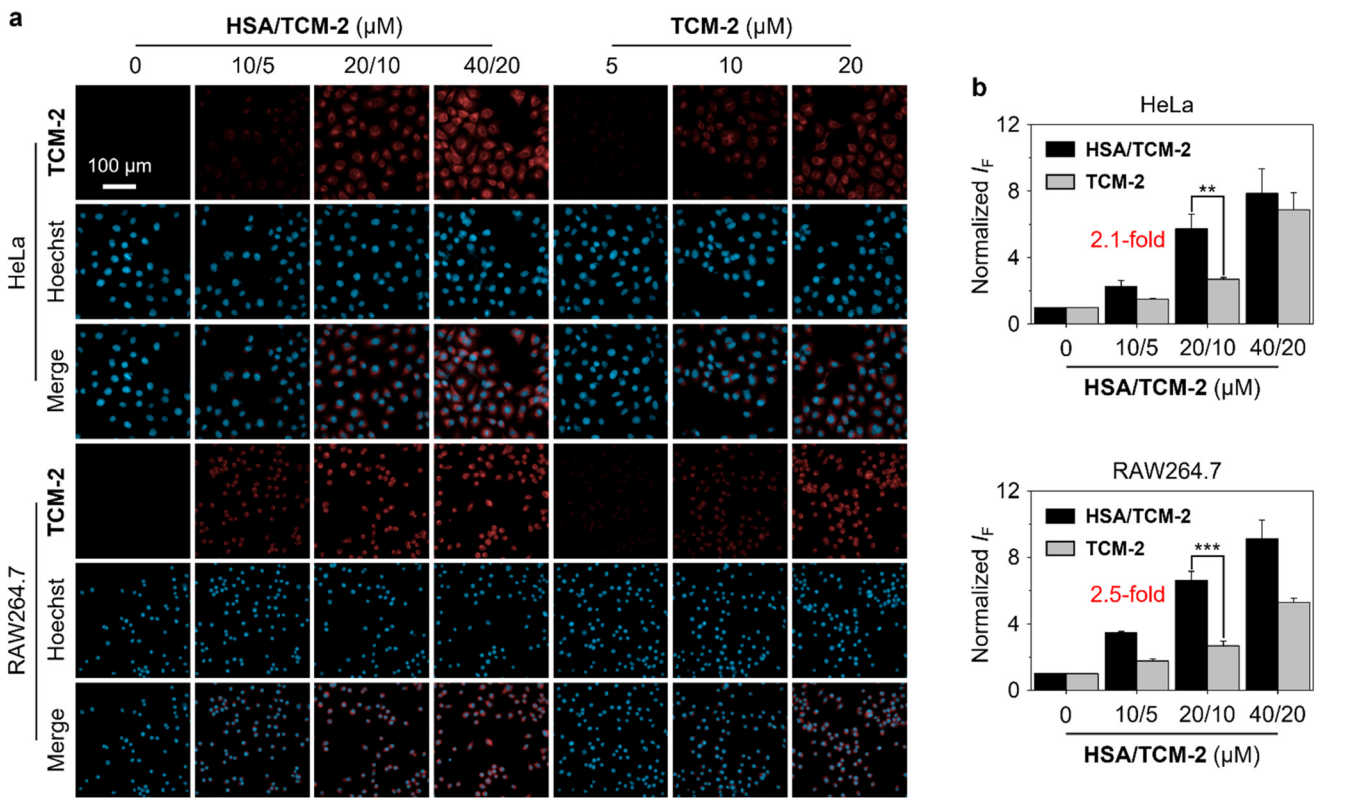

Fig. 4 Fluorescence imaging (a) and quantification of (b) of HeLa and RAW264.7 cells treated with **HSA/TCM-2** and **TCM-2** of different indicated concentrations (10–40/5–20 μM) in the presence of SIN-1 (500 mM) for 30 min. The excitation and emission wavelengths used are 561 nm and 570–650 nm, respectively. The cell nuclei were stained with Hoechst 33342. Error bars mean S. D. (n = 3). $^{**}P < 0.01$, $^{***}P < 0.001$.

This journal is © The Royal Society of Chemistry 2023

Open Access Article. Published on 22 May 2023. Downloaded on 12/6/2025 5:08:20 AM. This article is licensed under a Creative Commons Attribution 3.0 Unported Licence.

played a wide working pH range of 3–12 (Fig. S7a†), and selectivity over other ROS/RNS tested (Fig. S7b†).

Finally, the supramolecular probe was used for cell imaging. Two cell lines, HeLa (human cervical cancer) and RAW264.7 (mouse macrophage), were used. The cells were pretreated with SIN-1 (3-morpholinosydnonimine, a known $ONOO^-$ releasing agent) to upregulate intracellular $ONOO^-$ concentration, and were then treated with **HSA/TCM-2** and **TCM-2** of different concentrations for 30 min. We found that the fluorescence intensities of **HSA/TCM-2** were higher than those of **TCM-2** over the entire concentration range in both cells imaged (Fig. 4a and b). A remarkable 2.1-fold and 2.5-fold greater fluorescence of the supramolecular ensemble was determined at a **TCM-2** concentration of 10 μM in HeLa and RAW264.7 cells, respectively, suggesting the effectiveness of our HSA encapsulation strategy to enhance the sensing properties of fluorescent small-molecule probes in the complicated cellular environment.

The biological applications of small-molecule fluorescent probes are frequently limited by their low fluorescence brightness and insufficient biocompatibility due to molecular aggregation in biological media. Human serum albumin (HSA) is a biocompatible protein carrier suitable as a host for enhancing the imaging capacity of small-molecule probes, and as such a number of fluorescent dyes with HSA binding capacity have been developed.[35–38] Besides $ONOO^-$ sensing, we have demonstrated the applicability of HSA encapsulation for the enhanced fluorescence imaging of lysosomes based on receptor-directed endocytosis,[25] and intracellular glycosidases using super-resolution microscopy.[27] In addition, we have shown that this strategy could be extended to targeted fluorescence imaging of triple-negative breast cancer *in vivo*.[26] The use of other biomolecules such as amyloid β peptides to tune the fluorescence properties of small-molecule fluorescent probes has also been recently demonstrated.[39]

3. Conclusion

We have developed a supramolecular host–guest system formed with HSA, the most abundant protein in the human body, and a long-wavelength fluorogenic probe based on TCF. The probe when bound to a hydrophobic region of HSA exhibited a significantly enhanced sensitivity for $ONOO^-$ both in aqueous buffer solution and in cells. SAXS analysis combined with a competition assay corroborates that the probe is included in the **IIA** region of the HSA. This research offers insight into the simple construction of supramolecular systems with enhanced sensitivity for the detection of biologically relevant reactive species that exist at low concentrations in biological systems.

Conflicts of interest

The authors declare no conflict of interest.

Acknowledgements

The authors thank the National Natural Science Foundation of China (NSFC) (No. 92253306 and 82130099), the Shanghai Municipal Science and Technology Major Project (No. 2018SHZDZX03), the Fundamental Research Funds for the Central Universities (222201717003), the Programme of Introducing Talents of Discipline to Universities (B16017) and Open Funding Project of the State Key Laboratory of Bioreactor Engineering of East China University of Science and Technology for financial support. The Research Center of Analysis and Test of East China University of Science and Technology is gratefully acknowledged for assistance in analytical experiments. TDJ wishes to thank the University of Bath and the Open Research Fund of the School of Chemistry and Chemical Engineering, Henan Normal University (2020ZD01) for support.

References

1 M. Villanueva-Paz, L. Moran, N. Lopez-Alcantara, C. Freixo, R. J. Andrade, M. I. Lucena and F. J. Cubero, *Antioxidants*, 2021, **10**, 390.
2 C. Szabo, H. Ischiropoulos and R. Radi, *Nat. Rev. Drug Discovery*, 2007, **6**, 662–680.
3 R. Radi, *J. Biol. Chem.*, 2013, **288**, 26464–26472.
4 F. Wang, Q. Yuan, F. Chen, J. Pang, C. Pan, F. Xu and Y. Chen, *Front. Cell Dev. Biol.*, 2021, **9**, 742483.
5 Z. Liu, Z. Ren, J. Zhang, C. C. Chuang, E. Kandaswamy, T. Zhou and L. Zuo, *Front. Physiol.*, 2018, **9**, 477.
6 J. Li, J. Su, W. Li, W. Liu, B. T. Altura and B. M. Altura, *Neurosci. Lett.*, 2003, **350**, 173–177.
7 B. Guo, W. Shu, W. Liu, H. Wang, S. Xing, J. Chen and X. Zhang, *Sens. Actuators, B*, 2021, **344**, 130206.
8 M. K. Hulvey, C. N. Frankenfeld and S. M. Lunte, *Anal. Chem.*, 2010, **82**, 1608–1611.
9 W. Imaram, C. Gersch, K. M. Kim, R. J. Johnson, G. N. Henderson and A. Angerhofer, *Free Radicals Biol. Med.*, 2010, **49**, 275–281.
10 J. B. Li, L. Chen, Q. Wang, H. W. Liu, X. X. Hu, L. Yuan and X. B. Zhang, *Anal. Chem.*, 2018, **90**, 4167–4173.
11 X. Qin, F. Li, Y. Zhang, G. Ma, T. Feng, Y. Luo, P. Huang and J. Lin, *Anal. Chem.*, 2018, **90**, 9381–9385.
12 B. Wang, Y. Wang, Y. Wang, Y. Zhao, C. Yang, Z. Zeng, S. Huan, G. Song and X. Zhang, *Anal. Chem.*, 2020, **92**, 4154–4163.
13 Y. Bai, Y. Wang, L. Cao, Y. Jiang, Y. Li, H. Zou, L. Zhan and C. Huang, *Anal. Chem.*, 2021, **93**, 16466–16473.
14 S. Wang, L. Chen, P. Jangili, A. Sharma, W. Li, J.-T. Hou, C. Qin, J. Yoon and J. S. Kim, *Coord. Chem. Rev.*, 2018, **374**, 36–54.
15 W. T. Dou, H. H. Han, A. C. Sedgwick, G. B. Zhu, Y. Zang, X. R. Yang, J. Yoon, T. D. James, J. Li and X. P. He, *Sci. Bull.*, 2022, **67**, 853–878.

Open Access Article. Published on 22 May 2023. Downloaded on 12/6/2025 5:08:20 AM.
This article is licensed under a Creative Commons Attribution 3.0 Unported Licence.

16 H. H. Han, H. M. Wang, P. Jangili, M. Li, L. Wu, Y. Zang, A. C. Sedgwick, J. Li, X. P. He, T. D. James and J. S. Kim, *Chem. Soc. Rev.*, 2023, **52**, 879–920.
17 H. H. Han, H. Tian, Y. Zang, A. C. Sedgwick, J. Li, J. L. Sessler, X. P. He and T. D. James, *Chem. Soc. Rev.*, 2021, **50**, 9391–9429.
18 X. Chai, B. Li, C. Chen, W. Zhang, L. Sun, H. H. Han, Y. Zhang, S. Sun, J. Yang, J. Zhang and X. P. He, *Anal. Chem.*, 2023, **95**, 5747–5753.
19 M. Weber, H. H. Han, B. H. Li, M. L. Odyniec, C. E. F. Jarman, Y. Zang, S. D. Bull, A. B. Mackenzie, A. C. Sedgwick, J. Li, X. P. He and T. D. James, *Chem. Sci.*, 2020, **11**, 8567–8571.
20 H. H. Han, A. C. Sedgwick, Y. Shang, N. Li, T. Liu, B. H. Li, K. Yu, Y. Zang, J. T. Brewster II, M. L. Odyniec, M. Weber, S. D. Bull, J. Li, J. L. Sessler, T. D. James, X. P. He and H. Tian, *Chem. Sci.*, 2019, **11**, 1107–1113.
21 Y. Wu, H. H. Han, L. He, L. Li, Y. Zang, J. Li, X. P. He, Y. Ding, W. Cao and T. D. James, *Chem. Commun.*, 2023, **59**, 5051–5054.
22 T. Shao, X. Xu, L. Wang, Y. Shen, J. Zhao, H. Li, D. Zhang, W. Du, H. Bai, B. Peng and L. Li, *J. Innovative Opt. Health Sci.*, 2023, 2250039.
23 M. Li, H. Han, H. Zhang, S. Song, S. Shuang and C. Dong, *Spectrochim. Acta, Part A*, 2020, **243**, 118683.
24 R. Ramos, J. Bernard, F. Ganachaud and A. Miserez, *Small Sci.*, 2022, **2**, 2100095.
25 Y. Fu, H. H. Han, J. Zhang, X. P. He, B. L. Feringa and H. Tian, *J. Am. Chem. Soc.*, 2018, **140**, 8671–8674.
26 X. L. Hu, Q. Cai, J. Gao, R. A. Field, G. R. Chen, N. Jia, Y. Zang, J. Li and X. P. He, *ACS Appl. Mater. Interfaces*, 2019, **11**, 22181–22187.
27 X. Chai, H. H. Han, A. C. Sedgwick, N. Li, Y. Zang, T. D. James, J. Zhang, X. L. Hu, Y. Yu, Y. Li, Y. Wang, J. Li, X. P. He and H. Tian, *J. Am. Chem. Soc.*, 2020, **142**, 18005–18013.
28 A. C. Sedgwick, H. H. Han, J. E. Gardiner, S. D. Bull, X. P. He and T. D. James, *Chem. Commun.*, 2017, **53**, 12822–12825.
29 H. Y. Chen, D. Guo, Z. F. Gan, L. Jiang, S. Chang and D. W. Li, *Mikrochim. Acta*, 2018, **186**, 11.
30 X. Wang, L. Wang, T. Jin, K. Sun and J. Yang, *Sens. Actuators, B*, 2023, **375**, 132935.
31 D. Li, D. Lei, W. Ren, J. Li, X. Yang, Z. Cai, H. Duan and X. Dou, *Org. Biomol. Chem.*, 2023, **21**, 315–322.
32 A. A. Ksenofontov, P. S. Bocharov, K. V. Ksenofontova and E. V. Antina, *J. Mol. Liq.*, 2022, **345**, 117031.
33 H. Li, Q. Yao, J. Fan, J. Du, J. Wang and X. Peng, *Dyes Pigm.*, 2016, **133**, 79–85.
34 P. Shen, J. Hua, H. Jin, J. Du, C. Liu, W. Yang, Q. Gao, H. Luo, Y. Liu and C. Yang, *Sens. Actuators, B*, 2017, **247**, 587–594.
35 X. Chao, D. Yao, Y. Qi, C. Yuan and D. Huang, *Anal. Chim. Acta*, 2021, **1188**, 339201.
36 Y. F. Fan, F. Y. Wang, F. B. Hou, L. Wei, G. H. Zhu, D. F. Zhao, Q. Hu, T. Lei, L. Yang, P. Wang and G. B. Ge, *Chin. Chem. Lett.*, 2023, **34**, 1075571–1075574.
37 Y. Ke, J. Cao, J. Gong and N. Fu, *Sens. Actuators, B*, 2022, **352**, 131015.
38 D. Yuan, K. Pan, S. Xu and L. Wang, *Anal. Chem.*, 2022, **94**, 12391–12397.
39 A. C. Sedgwick, W.-T. Dou, J.-B. Jiao, L. Wu, G. T. Williams, A. T. A. Jenkins, S. D. Bull, J. L. Sessler, X.-P. He and T. D. James, *J. Am. Chem. Soc.*, 2018, **140**, 14267–14271.

This journal is © The Royal Society of Chemistry 2023